Full Papers

A Hybrid Scheme for the Solution of the Bivariate Spatially Distributed Population Balance Equation*

By *Menwer M. Attarakih*, *Hans-Jörg Bart***, and *Naim M. Faqir*

DOI: 10.1002/ceat.200500400

The advantages of the generalized fixed pivot technique as extended to mass transfer and the quadrature method of moments are hybridized to reduce the bivariate spatially distributed population balance equation describing the coupled hydrodynamics and mass transfer in liquid-liquid extraction columns. The key idea in the hybridization technique is to use the available moments furnished by the generalized fixed pivot technique to find the abscissa and weights for the Gaussian-quadrature based approach, in an attempt to evaluate the integrals over unknown droplet densities. To implement the quadrature method of moments efficiently, an explicit form for the abscissas and weights is derived based on the product-difference algorithm as described by McGraw [1]. The proposed technique is found to reduce the discrete system of partial differential equations from $2M_x + 1$ to $M_x + 2$, where M_x is the number of pivots or classes. The spatial variable is discretized in a conservative form using a couple of recently published central difference schemes. The numerical predictions of the detailed and reduced models are found to be almost identical, accompanied by a substantial reduction of the CPU time as a characteristic of the hybrid model.

1 Introduction

Liquid-liquid extraction columns (LLEC) are one of the major multiphase processes that call for population balance framework as a modeling tool, due to their dispersed nature. This framework would help in the optimal design of such equipment that has not yet been fulfilled, as they are still dependent on the time consuming and expensive scale-up methods from laboratory scale pilot plants. Such a realistic model for the simulation of typical LLECs should take into account the inevitable interactions between the column hydrodynamics and mass transfer. This is because the hydrodynamics and mass transfer are essentially determined by the behavior of the dispersed phase, which in turn is affected by the structure of the turbulent flow field as well as the column internal geometry [2–4]. These hydrodynamic and mass transfer interactions could be simulated using the population balances approach, taking into account the bivariate nature (with respect to droplet size and concentration) of the spatially distributed populations in the interacting liquid-liquid dispersions. In contrast to the previous spatially distributed population balance equation (SDPBE) describing the performance of LLECs [5], the present modeling approach allows the dynamic interaction of the mass transfer and fluid hydrodynamics by leaving it open to introduce a suitable model for predicting the interfacial tension, which changes as a function of solute concentration and markedly affects the breakage and coalescence rates [6].

In the present work, the state of any droplet is represented by a bivariate (joint) density function $n_{d,c_y}(d, c_y; t, z)$, where $n_{d,c_y}(d, c_y; t, z)\partial d\partial c_y$ represents the number of droplets having sizes and concentrations in the ranges $[d, d + \partial d] \times [c_y, c_y + \partial c_y]$ per unit volume of the contactor. This allows the discontinuous macroscopic (breakage and coalescence) and the continuous microscopic (interphase mass transfer) events to be coupled in a single SDPBE along with the transport equations describing the hydrodynamics and mass transfer of the continuous phase. These equations represent a system of mixed integro-partial and algebraic equations for which no analytical solution exists except for strongly simplified cases, and hence a numerical solution is required in general. A detailed numerical algorithm based on the quadrature method of moments (QMOM) and the generalized fixed-pivot technique as extended to mass transfer (GFPMT) is presented by Attarakih et al. [6]. The GFPMT could be viewed as a hybrid technique that couples the QMOM and the generalized fixed-pivot, which results in a two-population balance equation in terms of the droplet number and solute concentrations. Upon discretization using the GFPMT, this system of equations comprises a large system of conservation laws that is hyperbolically dominant. To reduce the dimensionality of the problem at hand a hybrid-

[*] Extended version of a paper presented at the DECHEMA/GVC-Jahrestagung 2004, October 12–14, Karlsruhe, Germany.

[**] Dr. M. M. Attarakih, Al-Balqa Applied University, Chem. Eng. Dept., P.O. Box 15008, 11134-Amman, Jordan; Prof. Dipl.-Ing. Dr. H.-J. Bart (author to whom correspondence should be addressed, bart@mv.uni-kl.de), TU Kaiserslautern, P.O. Box 3049, D-67653 Kaiserslautern, Germany; Prof. Dr. N. M. Faqir, University of Jordan, Chemical Eng. Dept., 11942, Amman, Jordan.

ization technique is proposed in this work that is still based on the QMOM and the GFPMT. This reduction technique retains the whole information furnished by the number concentration function and averages out the solute concentration coordinate without any simplifying assumptions regarding the form of the bivariate density function. The numerical results for the simulation of a pilot plant RDC column shows that there is a significant reduction in the CPU time when compared to the detailed model. In a separate work, validation of the model shows a good agreement between the predicted and experimental holdup and concentration profiles along the height of two simulated mini and pilot plant extraction columns; that is, Kühni and RDC columns, respectively [4].

2 Mathematical Model

The general SDPBE for describing the coupled hydrodynamics and mass transfer in LLECs in a one spatial domain could be written as [6][1]:

$$\frac{\partial n_{\mathrm{d,c_y}}(\psi)}{\partial t}+\frac{\partial[u_{\mathrm{y}} n_{\mathrm{d,c_y}}(\psi)]}{\partial z}+\sum_{\mathrm{i}=1}^{2}\frac{\partial[\dot{\zeta}_{\mathrm{i}} n_{\mathrm{d,c_y}}(\psi)]}{\partial \zeta_{\mathrm{i}}}= \frac{\partial}{\partial z}\left[D_{\mathrm{y}}\frac{\partial n_{\mathrm{d,c_y}}(\psi)}{\partial z}\right]+\frac{Q_{\mathrm{y}}^{\mathrm{in}}}{A_{\mathrm{c}}} n_{\mathrm{y}}^{\mathrm{in}}(d,c_{\mathrm{y}};t)\delta(z-z_{\mathrm{d}})+Y\{\psi\} \tag{1}$$

In this equation the components of the vector $\Psi = [d\, c_{\mathrm{y}}\, z\, t]$ are those for the droplet internal coordinates (diameter and solute concentration), the external coordinate (column height) z, and the time t, where the velocity vector along the internal coordinates is given by $\dot{\zeta} = [\dot{d}\dot{c}_{\mathrm{y}}]$. The source term $Y\partial\zeta$ represents the net number of droplets produced by breakage and coalescence per unit volume and unit time in the coordinates range $[\zeta, \zeta + \partial\zeta]$. The left hand side is the continuity operator in both the external and internal coordinates, while the first part on the right hand side is the droplet axial dispersion characterized by the dispersion coefficient D_{y}, which might be dependent on the energy dissipation and the droplet rising velocity [2]. The second term on the right hand side is the rate at which the droplets enter the LLEC with volumetric flow rate $Q_{\mathrm{y}}^{\mathrm{in}}$ that is perpendicular to the column cross-sectional area A_{c} at a location z_{d}, with an inlet number density $n_{\mathrm{y}}^{\mathrm{in}}$, and is treated as a point source in space. The dispersed phase velocity u_{y} relative to the walls of the column is determined in terms of the relative (slip) velocity with respect to the continuous phase and the continuous phase velocity u_{x} with respect to the walls of the column as follows:

$$\mathrm{u_y} = (1-\phi_{\mathrm{y}})\, u_{\mathrm{s}} - u_{\mathrm{x}} \tag{2}$$

The velocity u_{s}, appearing in the above equation, could be related to the single droplet terminal velocity u_{t} to take into account the droplet swarm (the effect of the dispersed phase hold up, ϕ_{y}) and the flow conditions in a specific equipment:

$$u_{\mathrm{s}} = K_{\mathrm{v}} u_{\mathrm{t}}(d, \boldsymbol{P}) \tag{3}$$

Where $\boldsymbol{P}$ is a vector of physical properties ($[\mu\ \rho\ \sigma\ ]$), and K_{v} is a slowing factor taking into account the effect of the column internal geometry on the droplet terminal velocity ($0 < K_{\mathrm{v}} \le 1$) [2, 4]. A useful guide for selecting the suitable droplet terminal velocity based on the shape of the droplet (rigid, oscillating, or circulating), and hence on the system physical properties, could be found in Gourdon et al. [7].

The solute concentration in the continuous phase c_{x} is predicted using a component solute balance on the continuous phase [6]:

$$\frac{\partial(\phi_{\mathrm{x}} c_{\mathrm{x}})}{\partial t}-\frac{\partial}{\partial z}\left(u_{\mathrm{x}}\phi_{\mathrm{x}} c_{\mathrm{x}}+D_{\mathrm{x}}\frac{\partial(\phi_{\mathrm{x}} c_{\mathrm{x}})}{\partial z}\right)= \frac{Q_{\mathrm{x}}^{\mathrm{in}} c_{\mathrm{x}}^{\mathrm{in}}}{A_{\mathrm{c}}}\delta(z-z_{\mathrm{y}})-\int_0^{\infty}\int_0^{c_{\mathrm{y,max}}}\dot{c}_{\mathrm{y}}\nu(d) n_{\mathrm{v,c_y}}(\psi)\partial d\partial c_{\mathrm{y}} \tag{4}$$

Note that the volume fraction of the continuous phase ϕ_{x} satisfies the physical constraint: $\phi_{\mathrm{x}} + \phi_{\mathrm{y}} = 1$. The left hand side of Eq. (4) as well as the first term on the right hand side, have the same interpretations as those for Eq. (1), however, with respect to the continuous phase. The last term appearing in Eq. (4) is the total rate of solute transferred from the continuous to the dispersed phase, where the liquid droplets are treated as point sources [8]. Note that Eq. (1) is coupled to the solute balance in the continuous phase given by Eq. (4) through the convective and the source terms.

3 Mass Transfer Coefficients

The individual mass transfer coefficients for the dispersed and continuous phases are found to be dependent on the behavior of the single droplet, i.e., with respect to whether it is stagnant, circulating or oscillating [9]. In the present work, the simplified model of Handlos and Baron [10] is used to predict the individual mass transfer coefficient for the dispersed phase, while the simple model based on the film coefficient equation, as recommended by Weinstein et al. [11], is used to predict that of the continuous phase. Accordingly, the suitable combination of these individual mass transfer coefficients results in the overall mass transfer coefficient K_{oy}, which can be used to predict the rate of change of solute concentration in the liquid droplet as expressed in terms of the droplet volume average concentration:

$$\frac{\partial c_{\mathrm{y}}(z,t)}{\partial t}=\frac{6K_{\mathrm{oy}}}{d}\left(c_{\mathrm{y}}^{*}(c_{\mathrm{x}})-c_{\mathrm{y}}(z,t)\right) \tag{5}$$

1) List of symbols at the end of the paper.

Note that K_{oy} may be a function of the droplet diameter d and time, depending on the internal state of the droplet; that is, whether it is circulating or behaving like a rigid sphere. The overall mass transfer coefficient is usually expressed using the two-resistance theory in terms of the individual mass transfer coefficients for the continuous and the dispersed phases [12] and $c_y^* = (\partial c_y/\partial c_x)c_x$.

4 The Hybridized Model

The model hybridization proceeds in two steps: First the quadrature method of moments (QMOM) is applied to integrate out the solute concentration after multiplying Eq. (1) by $c_y^m v(d)$ (with $m = 0$ and 1) and integrating it from 0 to $c_{y,max}$, which results in two coupled marginal densities: $n_d(d,z,t)$ and $q(d,z,t) = \int_0^{c_{y,max}} c_y v(d) n_{d,c_y}(\psi)\partial c_y$:

$$\frac{\partial n_d(d;z,t)}{\partial t} + \frac{\partial}{\partial z}\left[u_y n_d(d;z,t) - D_y \frac{\partial n_d(d;z,t)}{\partial z}\right] = \frac{Q_y^{in}}{A_c}\frac{n^{in}}{v_{in}}(t)\delta(z-z_y) + \pi_n(n_d,\bar{c}_y) \tag{6}$$

$$\frac{\partial q(d;z,t)}{\partial t} + \frac{\partial}{\partial z}\left[u_y q(d;z,t) - D_y \frac{\partial q(d;z,t)}{\partial z}\right] = \frac{Q_y^{in}}{A_c}\frac{c_y^{in} n^{in}(t)}{v_{in}}\delta(z-z_y) + \int_0^{c_{y,max}} \frac{\partial c_y}{\partial t} n_{d,c_y}(d,c_y;z,t)\partial c_y + \pi_q(n_d,q,\bar{c}_y) \tag{7}$$

The expressions of the source terms Π_n and Π_q are presented in detail by Attarakih et al. [6]. The application of the generalized fixed pivot technique starts by expanding the marginal density function (n_d, for example) as a sum of Dirac delta functions centered at the grid points (d_i) and then integrating the system of Eqs. (6) and (7) over the ith subdomain ($[d_{i-1/2}, d_{i+1/2}]$ $i = 1, 2, \ldots M_x$), which results in the following set of discrete PDEs:

$$\frac{\partial \phi_i(z,t)}{\partial t} + \frac{\partial}{\partial z}\left[u_{y,i}\phi_i(z,t) - D_y \frac{\partial \phi_i(z,t)}{\partial z}\right] = \frac{Q_y^{in}}{A_c}\phi_i^{in}(t)\delta(z-z_y) + \pi_{n,i} \tag{8}$$

$$\frac{\partial \Theta_i(z,t)}{\partial t} + \frac{\partial}{\partial z}\left[u_{y,i}\Theta_i(d;z,t) - D_y \frac{\partial \Theta_i(d;z,t)}{\partial z}\right] = \frac{Q_y^{in}}{A_c} c_y^{in}\phi_i^{in}(t)\delta(z-z_y) + \frac{6K_{oy,i}}{d_i}\left(\phi_i c_y^*(c_x) - \Theta_i\right) + \pi_{q,i} \tag{9}$$

$$\pi_{q,i} = \pi_{q,i}^b + \pi_{q,i}^c \tag{10}$$

$$\pi_{q,i}^b = -\Gamma_i\Theta_i + \sum_{k=i}^{M_x} \Pi_{i,k}\Gamma_k\Theta_k \tag{11}$$

$$\pi_{q,i}^c = -\Theta_i \sum_{k=1}^{Mmax(i)} \omega_{i,k}\frac{\phi_k}{v(d_k)} + \sum_{k=Kmin(i)}^{Kmax(i)} \sum_{j=Jmin(i,k)}^{Jmax(i,k)} \omega_{k,j}\Psi_{k,j}^{<i>} \left[\left(\frac{v(d_k)}{v(d_j)+v(d_k)}\right)\phi_j\Theta_k + \left(\frac{v(d_j)}{v(d_j)+v(d_k)}\right)\phi_k\Theta_j\right] \tag{12}$$

Where $f_i(z,t)$ and $T_i(z,t)$ are the total volume and solute concentrations in the ith subdomain and are given by:

$$\phi_i(z,t) = \int_{d_{i-1/2}}^{d_{i+1/2}} v(d) n_d(d;z,t)\partial d = v(d_i)N_i \tag{13}$$

$$\Theta_i(z,t) = \int_{d_{i-1/2}}^{d_{i+1/2}} v(d) q(d;z,t)\partial d = v(d_i)\bar{c}_i N_i \tag{14}$$

$$N_i(z,t) = \int_{d_{i-1/2}}^{d_{i+1/2}} n_d(d;z,t)\partial d \tag{15}$$

The mean solute concentration in the dispersed phase is obtained by combining the last two quantities as follows:

$$\bar{c}_y = \sum_{i=1}^{M_x} \Theta_i / \sum_{i=1}^{M_x} \phi_i \tag{16}$$

The ith interaction coalescence matrix $\Psi_{k,j}^{<i>}$ represents the effective number of coalescence events reporting in the ith subdomain with coalescence frequency ω, while $\Pi_{i,k}$ is an upper triangular breakage matrix that depends solely on the daughter droplet distribution. For details and implementation aspects of the GFP algorithm, the interested reader could refer to Attarakih et al. [13]. Note that the above source term takes into account the presence of mass transfer and could be reduced to the pure hydrodynamic case (Π_n) derived by Attarakih et al. [13] by setting $\bar{c}_i = 1$ in Eqs. (10–12). Note also that *Kmin(i)*, *Kmax(i)*, *Mmax(i)*, *Jmin(i, k)* and *Jmax(i, k)* represent the locations of the nonzero elements of the ith interaction matrix and depend on the droplet diameter grid structure once it becomes available [13].

To complete the mathematical model described above, boundary and initial conditions are required. Concerning the boundary conditions, we adopted those of Wilburn [14], while the initial conditions are taken as zero dispersed phase holdup and uniform solute concentration in the continuous phase. The inlet bivariate number density is taken as: $n_y^{in}(d,c_y;t) = n_y^{in}(d;t) \times c_y^{in}$, which means that all the inlet droplets have the same uniform solute concentration (zero in the present work).

The second step of the model hybridization consists of expanding the bivariate density function as $n_{d,c_y} = n_d(d)\delta(c_y - \bar{c}_y)$ using a one-point quadrature centered at the solute mean concentration $\bar{c}_y$. Making use of this expansion, multiplying both sides of Eq. (1) by $v(d)c_y$, and integrating with respect to c_y from zero to $c_{y,max}$ and with respect to d from d_{min} to d_{max} one can get the mean solute concentration in the dispersed phase:

$$\frac{\partial[\bar{c}_y\varphi_y]}{\partial t}+\frac{\partial}{\partial z}\left[\bar{c}_y\bar{F}(t,z)-D_y\frac{\partial[\bar{c}_y\phi_y]}{\partial z}\right]= \frac{Q_y^{in}}{A_c}\bar{c}_y^{in}\delta(z-z_y)+\bar{K}_{oy}\left(c_y^*(c_x)-\bar{c}_y\right) \quad (17)$$

$$\bar{F}_y=\int_{d_{min}}^{d_{max}}u_y(\bar{c}_y,d)v(d)n(d,z,t)\partial d\approx\sum_{j=1}^{N_q}u_y(\bar{c}_y,d_j)v(d_j)w_j \quad (18)$$

$$\bar{K}_{oy}=\int_{d_{min}}^{d_{max}}\frac{6K_{oy}(d,\bar{c}_y)}{d}v(d)n(d,z,t)\partial d\approx \sum_{j=1}^{N_q}\frac{6K_{oy}(d_j,\bar{c}_y)}{d_j}v(d_j)w_j \quad (19)$$

Note that the bivariate density function n_{d,c_y} is assumed to satisfy the regulatory conditions: $n_{d,c_y}\to 0$ as $(d,\ c_y)\to(d_{min},\ c_{y,min})$ and $(d,\ c_y)\to(d_{min},\ c_{y,max})$.

Now, the unclosed integrals appearing in the convective and mass transfer terms are evaluated using the QMOM based on the known moments of the marginal density $n(d,z,t)$, where the weights (w_j) and the abscissas (d_j) are found using the product-difference algorithm, as illustrated by McGraw [1], which for a two-point quadrature is reduced after lengthy but straight forward algebraic manipulations to the following analytical form:

$$d_j(t,z)=\frac{-b}{2}\pm\frac{1}{2}\sqrt{b^2-4c},\quad j=1,2 \quad (20)$$

$$w_j=\left(\frac{\sigma}{d_j-\tilde{\mu}_1}\right)^2\frac{\mu_0}{1+\left(\frac{\sigma}{d_j-\tilde{\mu}_1}\right)^2},\quad j=1,2 \quad (21)$$

where:

$$b=-\left(\tilde{\mu}_1+\frac{\tilde{\mu}_1^3-2\tilde{\mu}_1\tilde{\mu}_2+\tilde{\mu}_3}{\sigma^2}\right) \quad (22)$$

$$c=\tilde{\mu}_1\left(\frac{\tilde{\mu}_1^3-2\tilde{\mu}_1\tilde{\mu}_2+\tilde{\mu}_3}{\sigma^2}\right)-\sigma^2 \quad (23)$$

$$\sigma=\sqrt{\tilde{\mu}_2-\tilde{\mu}_1^2} \quad (24)$$

$$\tilde{\mu}_s=\frac{\mu_s}{\mu_0}=\frac{\int_{d_{min}}^{d_{max}}d^s n(d)\partial d}{\int_{d_{min}}^{d_{max}}n(d)\partial d},\ s=1,2,3 \quad (25)$$

The solution for the unknown marginal density ($n(d,z,t)$) is accomplished by the generalized fixed-pivot technique using the system of Eq. (8), where the required moments $(\mu_s=\int_{d_{min}}^{d_{max}}d^s n(d,z,t)\partial d=\sum_{m=1}^{M_x}d_m^s N_m, s=0,1,2,3)$ for the evaluation of the abscissa and weights (d_j and w_j) could be accurately predicted. The accuracy of predicting at least two moments (the zero and third moments) is one property of the generalized fixed pivot technique [13]. The first and second moments are usually predicted with high accuracy, allowing the two-point Gauss quadrature given above to evaluate the integrals appearing in Eqs. (18) and (19) very accurately. Although a two-point quadrature is used in this work, a three-point quadrature could also be used since most of the higher moments of the known distribution, $n(d,z,t)$, could be estimated with the desired accuracy.

5 Spatial Coordinate Discretization

Eqs. (4), (8), and (9), or (4), (8), and (17) represent a system of conservation laws that are coupled through the convective and source terms and are dominated by the convective term for typical values of D_y and u_y encountered in LLECs (Peclet No. $\approx 1\cdot10^3$ H–$2\cdot10^3$ H). Due to the dominance of the convective term, it is expected that the holdup profile of each class (φ_i) will move as a function of time along the column height with a steep front. So, accurate front tracking discretization approaches are to be used, such as the non-oscillatory first and second order central difference schemes. Let the ith convective flux be denoted as $F_i=u_{y,i}f_i$ and the staggering spatial grid: $z_{1\pm1/2}=z_1\pm\Delta z/2$, and the average cell holdup as $\phi_{i,1}=\int_{z_{1-1/2}}^{z_{1+1/2}}\phi_i(t,z)\delta z/\Delta z$. The convective flux is then discretized in conservative form using the Kurganov and Tadmor [15] central difference schemes (see [13] for a detailed spatial discretization algorithm), while the implicit Euler method by lagging the non-linear terms is used for time discretization.

6 Numerical Results and Discussion

To completely specify the problem, the following geometry, as given in Tab. 1, is used for a laboratory scale LLEC. The inlet feed is normally distributed with a mean droplet diameter of 3 mm and standard deviation of 0.5 mm. The inlet solute concentrations in the continuous and dispersed phases are taken as 50 and 0 kg/m^3, respectively, and the total flow rate of each phase is taken as $2.778\cdot10^{-5}$ m^3/s. The terminal droplet velocity is evaluated from the Vignes [16] correlation based on the procedure described by Gourdon et al. [7] using water-acetone-toluene as a chemical system (the physio-chemical properties of this system are available on the website: http://dechema.de/Extraktion), where the direction of mass transfer is from the continuous to the dispersed phase. The slowing factor, the dispersion coefficients, and the droplet interaction functions (droplet breakage and coalescence) are the same as those used by Schmidt et al. [17].

Table 1. RDC column geometry.

Column diameter [m]	0.15	Column height [m]	2.550
Stator diameter [m]	0.105	Dispersed phase inlet [m]	0.250
Rotor diameter [m]	0.090	Continuous phase inlet [m]	2.250
Compartment height [m]	0.030		

The initial condition is taken as zero (no dispersed phase present initially). All the numerical tests are conducted using a PC processor of 1.4 MHz speed and Compaq Visual FORTRAN version 6.6.

Fig. 1 shows the solute concentrations in the dispersed and continuous phases at steady state using a 2D grid of size 30×100, where the droplet active mechanism is droplet breakage at 250 rpm. It is clear, that both profiles as predicted by the detailed and reduced models are almost identical. This in fact elucidates the accuracy of the reduced model, and reveals clearly the efficiency of the generalized fixed-pivot technique for its ability to furnish the moments for the inversion of the moment problem to get the weights and the abscissas required to evaluate Eqs. (20) and (21). It is worthwhile to mention here that the accuracy of predicting the abscissas and weights, as given by Eqs. (20–25), depends on the accuracy of calculating the set of moments: $\mu_s, s = 0, 1, 2, 3$. To do that, a sufficient number of pivots (classes) should be used (around twenty or greater).

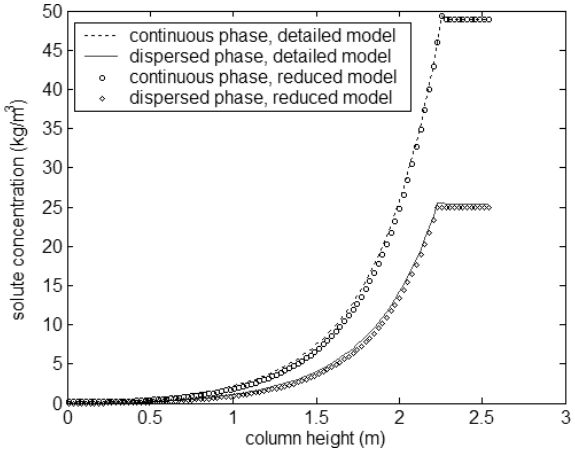

Figure 1. Steady state solute concentration as predicted by the detailed and reduced models for droplet breakage only at 250 rpm.

Fig. 2 shows again the same concentration profiles as in Fig. 1, however, both droplet breakage and coalescence are now active and hence the numerical difficulty is increased, as could be seen by referring to Eq. (12). It is also clear how both models produced identical results; however, at the expense of the computational time due to the reduced number of partial differential equations from $2M_x + 1$ to $M_x + 2$. Moreover, the simple form of Eq. (17) when compared to Eqs. (9–12) makes the hybridized model very attractive from the point of view of numerical implementation.

In Fig. 3, the variation of the holdup profiles as a function of the column height is depicted. The two profiles are clearly indistinguishable since Eq. (8) involves no hybridization, although there is some interaction between the hydrodynamics and mass transfer due to the coupling of Eqs. (8) and (17). Note that the hybridized model has an advantage over either the standard QMOM or the generalized fixed pivot technique in the way of its moderate recovery of the information furnished by solving the SDPBE. This is because it lies somewhere between two extreme cases: the complete averaging of the internal coordinates (the QMOM) and the detailed level of discretization as required by the generalized fixed pivot technique. For example, the present hybridized model presents a complete picture about the detailed column hydrodynamics, including the droplet volume density, as can be seen in Fig. 4a); however, it could not give a full picture about the solute distribution in the different droplet classes, as shown in Fig. 4b) as the detailed model does. In Fig. 4a), it is clear how the droplet distribution is shifted to the left as the droplets ascend up the column, due to breakage due to the increase in residence time and the reduction in surface tension (due to the increased solute concentration, as depicted in Figs. 1 and 4b)). Moreover, Steinmetz et al. [4], and Schmidt et al. [17] have extensively validated the present model experimentally for the coupled hydrodynamics and mass transfer. These authors have developed new correlations for droplet breakage, coalescence, as well as the effect of droplet swarm and the internal column geometry on the rising velocity of the droplets. Their simulated

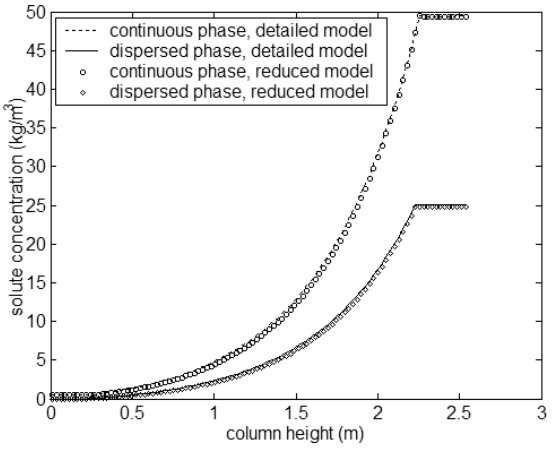

Figure 2. Steady state solute concentration as predicted by the detailed and reduced models for droplet breakage and coalescence at 250 rpm.

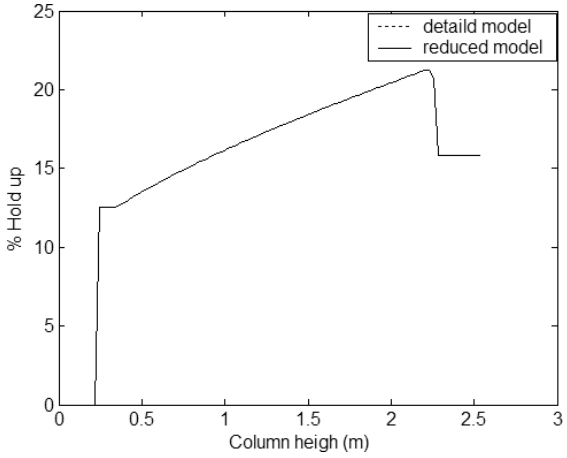

Figure 3. The dispersed phase hold up as predicted by the detailed and reduced models for droplet breakage only at 250 rpm.

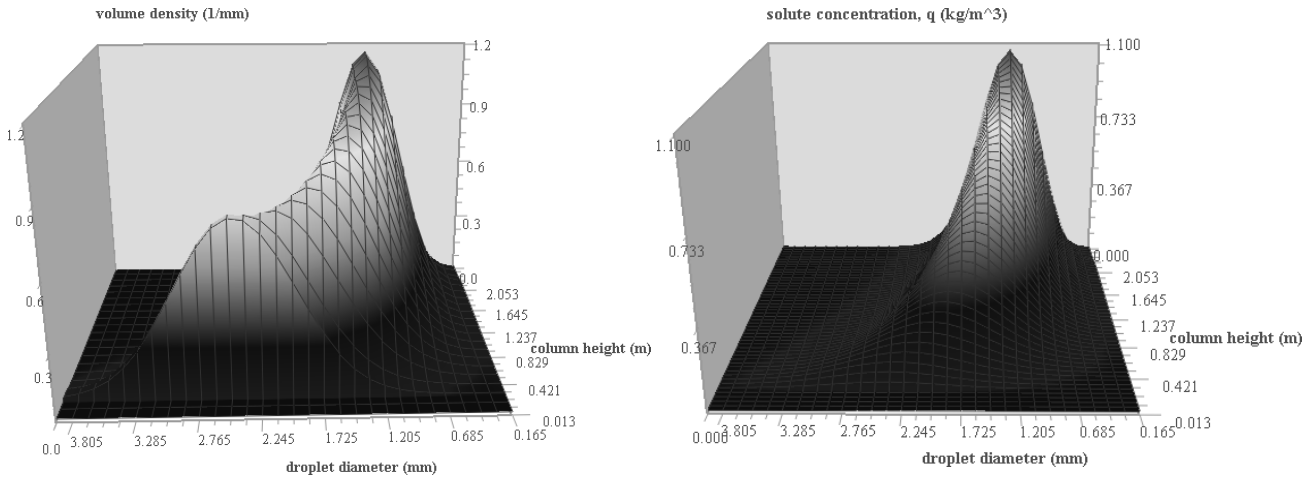

Figure 4. The droplet volume density as predicted by the reduced model for droplet breakage only at 250 rpm a). The solute concentration distribution as predicted by the detailed model for droplet breakage only at 250 rpm b).

holdup, mean droplet diameter, and the solute concentration profiles are very close to the experimental ones using different column sizes, geometries (an RDC of 100 and 152 mm diameters and a Kühni column of 32 mm diameter) and chemical systems (toluene-acetone-water and n-butyl acetate-acetone-water).

Fig. 5 shows the considerable reduction in the computational time when the hybridized model is used. This is because the dimensionality of the problem is reduced from $2M_x + 1$ to $M_x + 2$ partial differential equations. The surprising accuracy of the hybridized model is due to the detailed information that is included in the reduced model in terms of the moments of the known distribution, $n(d, z, t)$, without any simplifying assumptions regarding the shape of the distribution. The model is also capable of reflecting the effects of the solute concentration on the column hydrodynamics and visa versa, as is discussed in detail by Attarakih et al. [6] and Schmidt et al. [17].

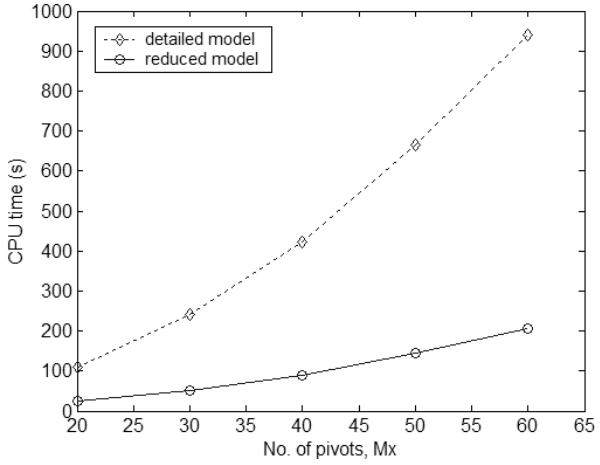

Figure 5. The CPU time requirements for the detailed and reduced models at 250 rpm.

7 Conclusions

- A comprehensive bivariate population balance model is presented to predict the behavior of spatially distributed population balances for LLECs by coupling the hydrodynamics and mass transfer through the breakage, coalescence frequencies, and the droplet rising velocity.
- The detailed and hybridized models presented in this work are found to produce almost identical predictions for the coupled hydrodynamics and mass transfer. The application of the QMOM to the hybridized model equations is found to be very effective in estimating the unclosed integrals, where a set of explicit abscissas and weights is derived using a two-point quadrature based on the product-difference algorithm.
- The reduced model shows a substantial reduction in the CPU time and an ease of numerical implementation when compared to the detailed one, without any loss of accuracy.

Acknowledgements

The authors would like to thank the DFG and DAAD for supporting this work.

Received: December 12, 2005

Symbols used

A_c	[m^2]	column cross sectional area
b, c	[–]	constants as defined by Eqs. (22) and (23)
$c_{y,max}$	[kg/m^3]	the maximum solute concentration attained (the equilibrium value)
$\bar{c}$	[kg/m^3]	average solute concentration

D	[m^2/s]	dispersion coefficient
d	[m]	droplet diameter
K_{oy}	[m/s]	overall mass transfer coefficient based on the dispersed phase
K_v	[–]	slowing factor that takes into account the effect of internal column geometry
M_x, N_q	[–]	number of pivots (classes) in the GFPMT and quadrature points respectively.
N_i	[1/m^3]	total number of droplets in the ith subdomain
N_q	[–]	number of quadrature points for droplet diameter
n_d, $c_y\partial/\partial c_y$	[1/m^3]	the number of droplets with d and $c_y \in [d, d + \partial d] \times [c_y, c_y + \partial c_y]$ per unit volume of the contactor
$\boldsymbol{P}$	[–]	vector of physical properties $[\mu\ \rho\ \sigma]$
Q	[m^3/s]	continuous or dispersed phase flow rate
$q(d, z, t)$	[–]	marginal density as defined by: $q(d;t,z) = \int_0^{c_{y,max}} c_y n_{d,c_y}(\psi)\partial c_y$
t	[s]	time
u	[m/s]	velocity
v	[m^3]	droplet volume
v_{in}	[Nm^3]	mean droplet volume of the inlet droplets
v(di)	[m^3]	characteristic volume of droplet in the ith subdomain
w	[–]	quadrature weight
z	[m]	space coordinate
$\int_0^{\infty}\int_0^{c_{y,max}} \dot{c}_y v(d) n_{v,c_y}(\psi)\partial d\partial c_y$	[kg/m^{3}s]	The totally quantity of solute transferred from all the droplet present in the continuous phase

Greek Symbols

Y	[1/s]	source term that represents the net number of droplet produced by breakage and coalescence
Γ	[1/s]	breakage frequency
$\Psi_{k,j}^{<i>}$	[–]	the ith interaction coalescence matrix
$\Pi_{i,k}$	[–]	an upper triangular breakage matrix that depends solely on the daughter droplet distribution
π	[–]	droplet interaction source terms as defined by Eqs. (10–12)
μ	[Pa s]	viscosity or distribution moment
μ_i	[–]	the ith moment of the distribution:
$\tilde{\mu}_i$	[–]	normalized moment as defined by Eq. (25)
ρ	[kg/m^3]	density
σ	[N/m]	interfacial tension
σ'_2	[–]	the variance of the distribution as defined by Eq. (24)
ϕ	[–]	phase holdup
φ_i	[–]	total volume concentration of droplets in the ith subdomain
ψ	[–]	internal and external coordinates vector ($[d\ c_y\ z\ t]$)
ω	[m^3/s]	coalescence frequency
Θ_i	[kg/m^3]	total solute concentration of droplets in the ith subdomain
$\dot{\zeta}$	[–]	internal coordinate velocity vector: $[\dot{d}\dot{c}_y]$

Subscripts

b, c	breakage and coalescence, respectively
x, y	continuous and dispersed phases, respectively
min, max	minimum and maximum, respectively

Superscripts

*	equilibrium

References

[1] R. McGraw, *Aerosol Sci. Tech.* **1997**, *27 (2)*, 255.
[2] G. Modes, H.-J. Bart, D. Rodrigue-Perancho, D. Bröder, *Chem. Eng. Tech.* **1999**, *22 (3)*, 231.
[3] M. Simon, S. Schmidt, H.-J. Bart, *Chem. Eng. Tech.* **2003**, *26 (7)*, 745. DOI: 10.1002/ceat.200306101
[4] T. Steinmetz, S. Schmidt, M. Attarakih, H.-J. Bart, in *Int. Solvent Extraction Conf., ISEC '05*, CD-ROM (ISBN 7–900692–02–9), China Acad. J. Electronic Publ. House, www.isec2005.org.ch, **2005**.
[5] S. Mohanty, *Review Chem. Eng.* **2000**, *16 (3)*, 199.
[6] M. M. Attarakih, H.-J. Bart, N. M. Faqir, *Chem. Eng. Sci.* **2006**, *61 (1)*, 113.
[7] C. Gourdon, G. Casamatta, G. Muratet, in *Liquid-Liquid Extraction Equipment* (Eds: J. C. Godfrey, M. J. Slater), John Wiley & Sons, New York **1994**.
[8] D. Ramkrishna, *Population Balances: Theory and Applications to Particulate Systems in Engineering*, Academic Press, San Diego **2000**.
[9] A. Kumar, S. Hartland, *Trans. Inst. Chem. Eng.* **1999**, *77* (part A), 372.
[10] A. E. Handlos, T. Baron, *AIChE J.* **1957**, *3 (1)*, 127.
[11] O. Weinstein, R. Semiat, D. R. Lewin, *Chem. Eng. Sci.* **1998**, *53 (2)*, 325.
[12] L. M. Ribeiro et al., *Comput. Chem. Eng.* **1997**, *21 (5)*, 543.
[13] M. M. Attarakih, H.-J. Bart, N. M. Faqir, *Chem. Eng. Sci.* **2004**, *59 (12)*, 2567.
[14] N. P. Wilburn, *Ind. Eng. Chem. Fundam.* **1964**, *3 (3)*, 189.
[15] A. Kurganov, E. Tadmor, *J. Com. Phys.* **2000**, *160 (1)*, 241.
[16] A. Vignes, *Genie Chimique* **1965**, *93 (5)*, 129.
[17] A. S. Schmidt et al., *Chem. Eng. Sci.* **2005**, *61 (1)*, 246.

